Volume 15
Number 27
21 July 2024
Pages 10251–10672

Chemical Science

rsc.li/chemical-science

ISSN 2041-6539

ROYAL SOCIETY OF CHEMISTRY

EDGE ARTICLE

Marcus W. Drover *et al.*

Oxidatively-induced C(sp^3)–C(sp^3) bond formation at a tucked-in iron(III) complex

Chemical Science

ROYAL SOCIETY OF CHEMISTRY

EDGE ARTICLE

View Article Online
View Journal | View Issue

Cite this: *Chem. Sci.*, 2024, **15**, 10359

All publication charges for this article have been paid for by the Royal Society of Chemistry

Received 20th May 2024
Accepted 6th June 2024

DOI: 10.1039/d4sc03292f

rsc.li/chemical-science

Oxidatively-induced C(sp^3)–C(sp^3) bond formation at a tucked-in iron(III) complex†

Joseph A. Zurakowski, [ab] Connor S. Durfy, [a] Noah B. Stocek,[c] Giovanni Fanchini [ac] and Marcus W. Drover *[a]

Carbon–carbon (C–C) bond formation is a cornerstone of synthetic chemistry, relying on routes such as transition-metal mediated cross-coupling for the introduction of new carbon-based functionality. For {[M]$^{n+}$–C} (M = metal) structural units, studies that offer well-defined relationships between metal oxidation state, hydrocarbon strain, and {[M]$^{n+}$–C} bond thermochemistry are thus informative, providing a means to reliably access new product classes. Here, we show that one-electron oxidation of the iron tucked-in complex [(η^6-C_5Me_4=CH_2)Fe(d*n*ppe)] (d*n*ppe = 1,2-bis(di-*n*-propylphosphino)ethane) results in C(sp^3)–C(sp^3) bond formation giving unique {Fe_2} dimers. Freeze-quenched CW X-band EPR spectroscopy allowed for spectroscopic identification of the reactive [(η^6-C_5Me_4=CH_2)Fe(d*n*ppe)]$^+$ intermediate. Density functional theory (DFT) calculations reveal a primarily Fe-centered radical and a weak {[Fe]–C} bond ($BDE_{[Fe]-C}$ = 24.5 kcal mol^{-1}, *c.f.* $BDE_{C-C(ethane)}$ = 90 kcal mol^{-1}). For comparison, a structurally analogous Fe(III) methyl complex was prepared, [Cp*Fe(d*n*ppe)(CH_3)]$^+$ (Cp* = $C_5Me_5^-$), where C(sp^3)–C(sp^3) coupling was not observed, consistent with a larger calculated $BDE_{[Fe]-C}$ value of 47.8 kcal mol^{-1}. These data are analogized to the simple hydrocarbons ethane and cyclopropane, where a strain-induced BDE_{C-C} decrease of 33 kcal mol^{-1} is witnessed on cyclization.

Introduction

Carbon–carbon (C–C) bond forming reactions are a cornerstone of synthetic chemistry. Most pharmaceutically active compounds contain a C–C bond, along with countless materials relevant to industry and everyday life. It thus comes as no surprise that transition metal mediated C–C bond forming reactions have been the focus of two Nobel prizes.[1,2] Using transition metals, one can form C–C bonds through cross-coupling – a sequence that proceeds *via* stepwise oxidative addition, transmetalation, and reductive elimination.[3] In recent years, there has been a surge of reports that have driven such transformations using electro-[4–7] or photochemistry;[8–11] many of these studies have focused on cheaper and more abundant base transition elements as feedstocks.[12]

Reductive elimination is the main step associated with C–C bond formation.[13] When reductive elimination from {[M]$^{n+}$–C} is unfavourable and prohibits C–C bond generation, oxidation of the metal-center can be used to induce so called oxidatively-induced reductive elimination (ORE; Fig. 1A).[14–16] In this way, oxidation increases the tendency to undergo elimination (*e.g.*, homolytic bond cleavage), thus returning the metal to a stable d-electron count.[17,18]

Sanford and co-workers have shown that one-electron oxidation of [(^{t}Bu$_2$bpy)Pd^{III}(CH_3)$_2$]$^+$ (^{t}Bu$_2$bpy = 4,4′-di-*tert*-butyl-2,2′-bipyridine) results in C(sp^3)–C(sp^3) reductive elimination of ethane (CH_3CH_3) from an intermediate {[Pd^{IV}]-(CH_3)$_3$} species (Fig. 1A).[19] Similarly, Baik, Chang, and co-workers showed that oxidation of an Ir(III) complex to Ir(IV) led to a 19 kcal mol^{-1} reduction in the barrier associated with reductive elimination in a C–H arylation reaction.[20] These examples illustrate the power of ORE in C–C bond formation, providing opportunities for otherwise unfavourable bond construction.

Of {[M]$^{n+}$–C} organometallics, sandwich complexes ([Cp/Cp*]$_2$M; Cp = $C_5H_5^-$; Cp* = $C_5Me_5^-$) represent a well-studied area owing to robust syntheses and product stability.[21,22] Lesser studied, however, are related "tucked-in" complexes, where a H^+/$H^•$/H^- from the Cp*–CH_3 ligand has been removed, encouraging high reactivity.[23] This is especially true for first row late transition elements. As a salient example, it was reported that the ferrocenyl carbocation, [((η^6-C_5Me_4)=CH_2)Fe(Cp*)]$^+$ is reactive at temperatures >−82 °C.[24–26]

[a]*Department of Chemistry, Western University, 1151 Richmond Street, London, ON, N8K 3G6, Canada. E-mail: marcus.drover@uwo.ca*

[b]*Department of Chemistry and Biochemistry, University of Windsor, 401 Sunset Avenue, Windsor, ON, N9B 3P4, Canada*

[c]*Department of Physics and Astronomy, Western University, 1151 Richmond Street, London, ON, N6A 3K7, Canada*

† Electronic supplementary information (ESI) available: Experimental procedures, spectroscopic data, computational details. CCDC 2341812. For ESI and crystallographic data in CIF or other electronic format see DOI: https://doi.org/10.1039/d4sc03292f

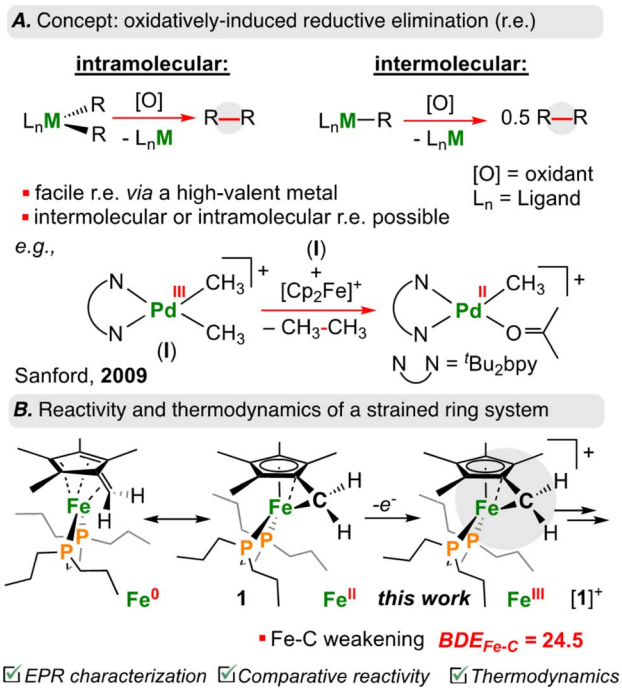

Fig. 1 (A) Overview of intra/intermolecular oxidatively induced reductive elimination with transition metals. (B) Decrease in BDE_{C-C} in cyclopropane upon oxidation, and this work.

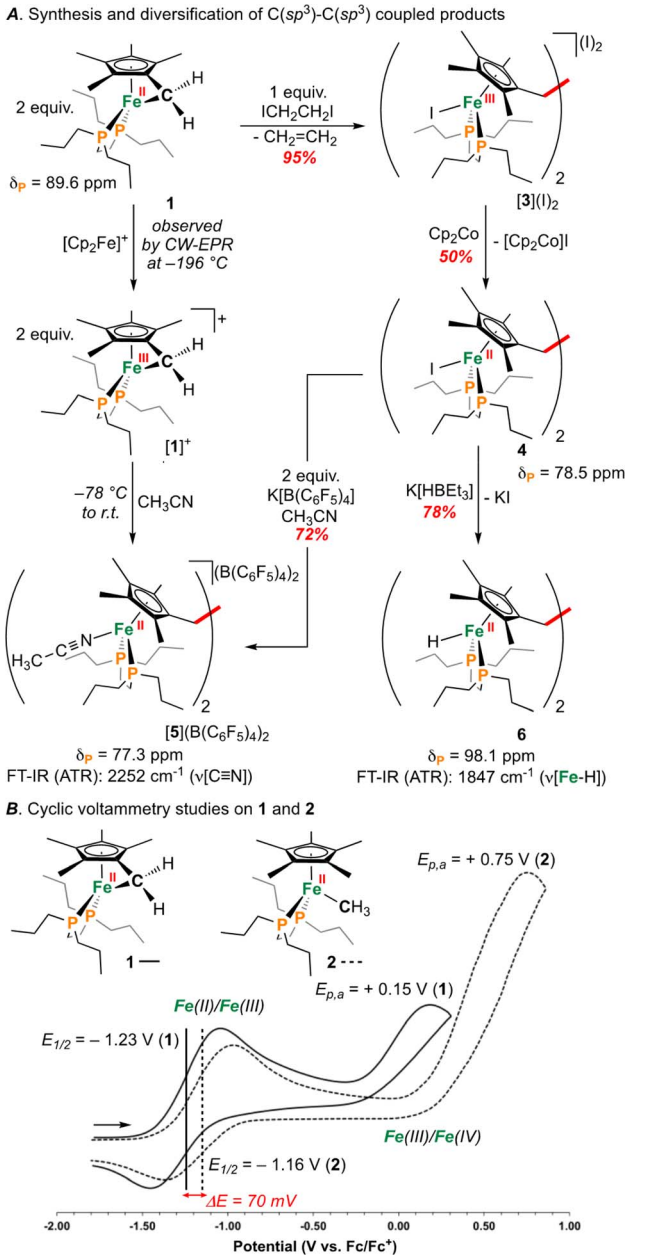

Fig. 2 (A) Synthesis of $[1]^+$ and $C(sp^3)$–$C(sp^3)$ coupled products. (B) Cyclic voltammograms for **1** and **2**.

Recently, we reported the first example of an Fe diphosphine tucked-in complex, $[(\eta^6\text{-}C_5Me_4)\text{=}CH_2)Fe(d\textit{n}ppe)]$ (d*n*ppe = 1,2-bis(di-*n*-propylphosphino)ethane) (**1**) (Fig. 1B) and its reactivity with electrophiles including CO_2, $HBCy_2$ (Cy = cyclohexyl), Br–Au^I-PPh_3, benzaldehyde, and $B(C_6F_5)_3$.[27] Herein, we examine the redox behaviour of **1** using electrochemical, photochemical, and chemical means (Fig. 2A). Oxidation of the Fe-center in **1** led to rapid $C(sp^3)$–$C(sp^3)$ formation between CH_2 groups of the η^6-C_5Me_4=CH_2 ligand. Model studies and theoretical calculations were used to rationalize iron–carbon {$[Fe]^{n+}$–C} bond strength (*i.e.*, bond dissociation energy (BDE)) as a function of both iron oxidation state and ring-strain. These observations are analogized to cyclic organic compounds (*e.g.*, cyclopropane) that also bear weak C–C bonds due to strain – a characteristic that has been leveraged for oxidatively-induced functionalization.[28,29]

Results and discussion

An investigation into the oxidative chemistry of **1** was commenced by means of cyclic voltammetry (CV). Scanning from −1.90 V to +0.50 V in THF showed a quasi-reversible feature at $E_{1/2}$ = −1.23 V (i_P^{red}/i_P^{ox} = 0.89 at 200 mV s^{-1}; Fig. S43†)[30] and an irreversible feature at $E_{p,a}$ = +0.15 V *vs.* Fc/Fc^+ (Fc = ferrocene) (Fig. 2B); these are assigned as Fe(II/III) and Fe(III/IV) events, respectively.[31] Varying the scan rate from 50 to 500 mV s^{-1} did not change voltammogram shape (Fig. S44†). For other known Fe(II) half-sandwich complexes, $[Cp^*Fe^{II}(dppe)(X)]$ (dppe = 1,2-bis(diphenylphosphino)ethane; X = H, CH_3, F, Cl, Br, I), the Fe(II/III) couple was found to be $-0.54 > E_{1/2} > -0.88$ V, indicating the $E_{1/2}$ value for **1** to be comparably cathodically shifted.[32,33] To probe the effect of hydrocarbon strain on electrochemical oxidation, an analogous $\{[Fe^{II}]\text{–}CH_3\}$ complex $[Cp^*Fe^{II}(d\textit{n}ppe)(CH_3)]$ (**2**) (Fig. 2B) was examined.[34] Compound **2** showed a reversible feature at $E_{1/2}$ = −1.16 V with i_P^{red}/i_P^{ox} near 1.00 at 200 mV s^{-1} (Fig. S45†), and an irreversible feature at $E_{p,a}$ = +0.35 V *vs.* Fc/Fc^+ in THF, indicating that the tucked-in η^6-C_5Me_4=CH_2 ligand contributes to a 70 mV cathodic shift in the Fe(II/III) couple. For both **1** and **2**, the Fe(III/IV) couple was irreversible – a reported outcome for $[Cp^*Fe(diphosphine)(CH_3)]^+$-type complexes.[32]

As a result of our observations from the CV data, complex **1** was next exposed to 1 equiv. of $[Cp_2Fe]B(C_6F_5)_4$ at 25 °C (Fig. 2A)

in CH_3CN. Monitoring this reaction by $^{31}P\{^1H\}$ NMR spectroscopy showed the formation of diamagnetic products in the range of *ca.* $\delta_P = 78$ ppm, consistent with complexes of the type $[Cp^*Fe(diphosphine)(NCCH_3)]^+$.[33] This hypothesis was further supported by FT-IR spectroscopy, providing a band at $\nu(C{\equiv}N) = 2252\ cm^{-1}$ (*c.f.*, $\nu(C{\equiv}N) = 2234\ cm^{-1}$) for $[Cp^*Fe(dnppe)(NCCH_3)]^+$, prepared independently (*vide infra*; $[\mathbf{7}]^+$) (Fig. S28†).

Supposing the main product from oxidation of **1** to be the C(sp^3)–C(sp^3) coupled $\{\mu\text{-}H_2CCH_2{}^-\}$ dimer, $[\{\eta^5\text{-}C_5Me_4\text{–}(\mu\text{-}CH_2)\}Fe^{II}(dnppe)(NCCH_3)]_2{}^{2+}$ ($[\mathbf{5}]^{2+}$), the redox behaviour of **1** was probed in the presence of 4 mL of THF with 100 μL CH_3CN added.[35] Consistent with an electrochemical–chemical (EC) reaction (onwards reactivity), scanning oxidatively from −2.00 to +1.00 V showed the previously discussed quasi-reversible couple at $E_{1/2} = -1.23$ V, with a decreased value of $i_P^{red}/i_P^{ox} = 0.62$ (*c.f.*, 0.89 in THF at 200 mV s^{-1}). In addition to the observed signature for **1**, an additional wave at $E_{1/2} = -0.16$ V was assigned to the Fe(II/III) couple of $[\mathbf{5}]^{2+}$, confirmed through independent preparation (*vide infra*; Fig. S51†).

Outlining an alternative preparation of $[\mathbf{5}]^{2+}$, we envisaged treatment of **1** with a halide-based oxidant to initiate C(sp^3)–C(sp^3) coupling, followed by halide abstraction in CH_3CN (Fig. 2A). Diiodoethane (ICH_2CH_2I), previously shown to oxidize $\{Fe(diphosphine)_x\}$ complexes,[36] was selected as the candidate oxidant, supplying iodide groups that could later be removed. In accord, exposure of **1** to 1 equiv. of ICH_2CH_2I showed an immediate colour change from orange to dark red (Fig. 2A). Analysis by $^{31}P\{^1H\}$ NMR spectroscopy, however, showed an absence of signals, suggestive of paramagnetism. Growth of crystals from a THF solution layered with pentane at −35 °C overnight provided material appropriate for an Evans method measurement, giving $\mu_{eff} = 2.66\ \mu_B$ (298 K, $CDCl_3$), falling within the expected range of a molecule containing two unpaired electrons. Further analysis by single-crystal X-ray diffraction (scXRD) revealed a connectivity map that supported a dimeric structure of $[\{\eta^5\text{-}C_5Me_4\text{–}(\mu\text{-}CH_2)\}Fe^{III}(dnppe)(I)]_2(I)_2$ ($[\mathbf{3}](I)_2$) (Fig. S54†). This molecule features a bridging $\{\mu\text{-}H_2CCH_2\text{–}\}$ unit that links two $\{(C_5Me_4\text{–}(CH_2))Fe^{III}(dnppe)(I)\}$ moieties. Consistent with the μ_{eff} value obtained from Evans method and the two exogeneous iodide counteranions observed by scXRD, both Fe-centers are formally Fe(III). High-resolution electrospray ionization mass-spectrometry (HRMS-ESI) additionally provides a signal for $[\mathbf{3}]^+$ at $m/z = 1158.299$ (calcd. $m/z = 1158.293$).

Formation of $[\mathbf{3}](I)_2$ is a four-electron process involving two successive oxidations of **1**. Considering the Fe(II) resonance contributor for **1** (Fig. 1B), oxidation leads to homolytic bond cleavage, forming an $S = 1$ Fe(II) center[37] and a $\{C_5Me_4\text{–}(\cdot CH_2)\}$ radical (*vide infra*). Recombination of two $\{C_5Me_4\text{–}(\cdot CH_2)\}$ radicals results in C(sp^3)–C(sp^3) bond formation. Iodide coordination and subsequent oxidation to Fe(III) (by excess ICH_2CH_2I) thus provides the observed product $[\mathbf{3}](I)_2$ (Fig. 2A). To provide the Fe(II) complex $[\{\eta^5\text{-}C_5Me_4\text{–}(\mu\text{-}CH_2)\}Fe^{II}(dnppe)(I)]_2$ (**4**), 0.5 equiv. of ICH_2CH_2I was added to **1** (to preclude oxidation from Fe(II) to Fe(III)). However, this reaction resulted in mixtures of products, with at least two $^{31}P\{^1H\}$ resonances appearing in the range of **4** (δ_P = *ca.* +80 ppm), unreacted **1** ($\delta_P = +89.6$ ppm), and free d*n*ppe ($\delta_P = -28.3$ ppm) (Fig. S30†).

As an alternative route towards **4**, reduction of $[\mathbf{3}](I)_2$ was explored using cobaltocene ($[Cp_2Co]$). Addition of 2 equiv. of $[Cp_2Co]$ to a THF solution of $[\mathbf{3}](I)_2$ produced an insoluble yellow precipitate and a purple supernatant over 3 h. Extraction of the purple product into toluene and analysis by NMR spectroscopy revealed a diamagnetic product. By $^{31}P\{^1H\}$ NMR spectroscopy, one signal at $\delta_P = +78.5$ ppm was observed, standard of $[Cp^*Fe^{II}(dnppe)(halide)]$-type compounds (*e.g.*, for halide = Cl, $\delta_P = +79.4$ ppm).[34] Analysis of the ^1H NMR spectrum also revealed a characteristic signal for the bridging $\{\mu\text{-}H_2CCH_2\text{–}\}$ moiety ($\delta_H = 2.57$ ppm) as well as two pairs of signals for the unsymmetric methyl $\{\eta^5\text{-}C_5\underline{Me}_4\}$ groups ($\delta_H = 1.89$ and 1.82 ppm). Crystals of **4** were grown from slow evaporation of a benzene solution overnight; analysis by scXRD confirmed its structural identity as $[\{\eta^5\text{-}C_5Me_4\text{–}(\mu\text{-}CH_2)\}Fe^{II}(dnppe)(I)]_2$ (**4**) (Fig. 3). Offering context, a Cambridge Structural Database (CSD) search provides fewer than 5 examples of structurally-authenticated Cp*-based compounds featuring a bridging $\{\text{–}H_2CCH_2\text{–}\}$ unit.[24,38–43] Using pre-formed ligand constructs, Wang and co-workers reported a set of polymeric Ir complexes bridged by $\{C_5Me_4\text{–}(CH_2)_n\text{–}C_5Me_4\}$ (n = 2, 3, 4);[40] while Brintzinger and co-workers synthesized monometallic complexes of the type $[(C_5Me_4\text{–}(CH_2)_2\text{–}C_5Me_4)MCl_2]$ (M = Ti, Zr).[41] Another example has been accessed by Cp*$\{H^\cdot\}$ removal – Severin and co-workers utilized $[OAl(C_6F_5)_3]^{\cdot-}$ in the presence of $Al(C_6F_5)_3$ to perform H-atom abstraction of $[Cp^*_2Fe]$, generating a $[(\eta^5\text{-}C_5Me_4)(\cdot CH_2)]Fe(Cp^*)]$ radical,[38] which dimerized to give $[\{\eta^5\text{-}C_5Me_4\text{–}(\mu\text{-}CH_2)\}Fe^{II}(Cp^*)]_2$. This example, however, does not require Fe oxidation nor does it inform on the relationship between iron-ring-strain and C–C coupling.

Compound **4** is a viable candidate for halide abstraction in CH_3CN. Reaction of a CH_3CN solution of **4** with 2 equiv. K$[B(C_6F_5)_4]$ (Fig. 2A) produced an immediate colour change from purple to orange. After workup, FT-IR (ATR) spectroscopic analysis showed a stretch at $\nu(N{\equiv}C) = 2252\ cm^{-1}$, corroborating formation of $[\{\eta^5\text{-}C_5Me_4\text{-}(\mu\text{-}CH_2)\}Fe^{II}(dnppe)(NCCH_3)]_2[\text{-}B(C_6F_5)_4]_2$ ($[\mathbf{5}](B(C_6F_5)_4)_2$). The ^1H NMR spectrum of $[\mathbf{5}]^{2+}$ also showed the expected inequivalent $\{\eta^5\text{-}C_5\underline{Me}_4\}$ signals

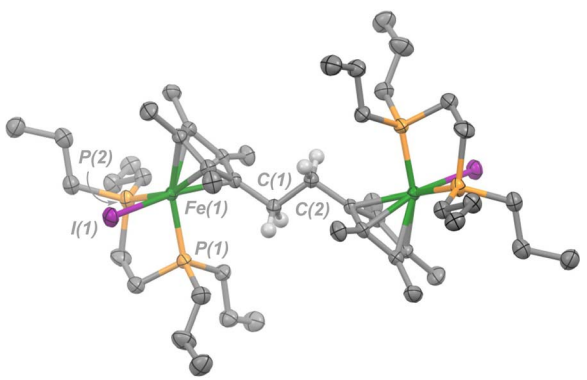

Fig. 3 Molecular structure of **4** with ellipsoids drawn at 50% probability. Hydrogen atoms omitted except for those on C(1) and C(2). Solvent molecule (benzene) has been omitted for clarity.

($\delta_H = 1.63$ and 1.48 ppm), a {μ-CH_2} signal ($\delta_H = 2.22$ ppm), and a peak for [Fe]-NCC<u>H</u>$_3$ ($\delta_H = 2.41$ ppm; *c.f.*, $\delta_H = 1.91$ ppm for [Cp*Fe(d*n*ppe)($NCCH_3$)]$^+$ ([**7**]$^+$)). Comparison of the FT-IR spectra for the reaction between **1** and [Cp_2Fe]$B(C_6F_5)_4$, [**5**]$^{2+}$, [**7**]$^+$, and neat CH_3CN, confirmed that [**5**]$^{2+}$ was formed from oxidation of **1** (Fig. 4) with an observed stretch at ν(N≡C) = 2252 cm^{-1}. Notably, the combination band for neat CH_3CN (ν = 2300 cm^{-1}) also disappears upon CH_3CN coordination.[44,45] In addition to our observations from IR spectroscopy, a THF solution of **4** exposed to 100 μL of CH_3CN and analyzed by CV displayed a predominant wave at $E_{1/2} = -0.16$ V, akin to the voltammogram acquired from the addition of 100 μL CH_3CN to **1**, noted above (Fig. S51†).

Compound **4** is also a valuable synthon for clean access to dimeric iron hydrides. For example, exposure of a THF solution of **4** to 2 equiv. of K[$HBEt_3$] led to clean formation of the bis-hydride complex [{η^5-C_5Me_4–(μ-CH_2)}Fe^{II}(d*n*ppe)(H)]$_2$ (**6**) (Fig. 2A).[46] By ^{1}H NMR spectroscopy, the bridging {μ-H_2CCH_2–} group was located at $\delta_H = 2.62$ and the inequivalent {η^5-C_5<u>Me</u>$_4$} signals were observed at $\delta_H = 2.05$ and 1.96 ppm. Successful [Fe]–H formation was further established by locating the [Fe]–H signal as a triplet at $\delta_H = -17.81$ ppm ($^2J_{H-P} = 70.2$ Hz) (*c.f.*, $\delta_H = -17.90$ ppm ($^2J_{H-P} = 70.2$ Hz) for the monomeric [Cp*Fe(d*n*ppe)(H)]).[34] FT-IR spectroscopy also revealed a characteristic ν(Fe–H) stretch at 1847 cm^{-1}.

Having characterized the terminal C(sp^3)–C(sp^3) coupled product, we next sought to characterize the reactive oxidized precursor, [**1**]$^+$. Oxidation of **1** was thus carried out in 2-MeTHF using [Cp_2Fe]$^+$ at −78 °C. Following 5 min of reaction time, freeze-quenched continuous wave (CW) X-band EPR spectroscopy provided a spectrum with rhombic symmetry (g = [2.0004, 2.0526, 2.2134]) (Fig. 5A) – this represents the first example of a spectroscopically characterized Fe(III) tucked-in complex by EPR. Compound [**1**]$^+$ can likewise be photochemically generated in a 2-MeTHF glass using **1** and a 405 nm laser (350 mW mm^{-2}) following 10 min of irradiation (Fig. 5B). To provide a comparative basis, the {[Fe^{III}]–CH_3} complex [**2**]$^+$ was also prepared by reaction of **2** with 1 equiv. of [Cp_2Fe]$^+$ in 2-MeTHF at −78 °C. By CW X-band EPR spectroscopy, a rhombic signal was also observed (g = [1.9827, 2.0450, 2.3968]) (Fig. 5A), again consistent with an $S = 1/2$ Fe(III) radical species ([**2**]$^+$).[47] The g_{max} shift between compounds [**1**]$^+$ and [**2**]$^+$ is attributed to a difference in geometry about Fe. For [**1**]$^+$, g-values are all greater than 2.0 with a spread of 0.05 to 0.16 – characteristic of the unpaired electron predominately residing in a d_{z^2} orbital.[48] For [**2**]$^+$,

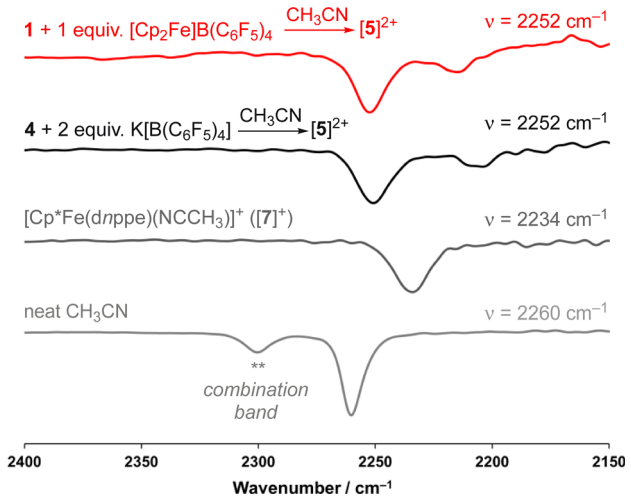

Fig. 4 Enhanced view of the region between 2400–2150 cm^{-1} for the FT-IR (ATR) spectra for the reaction between **1** and 1 equiv. of [Cp_2Fe]$B(C_6F_5)_4$ (red), [**5**]$^{2+}$ (black), [**7**]$^+$ (dark grey), and neat CH_3CN (light grey).

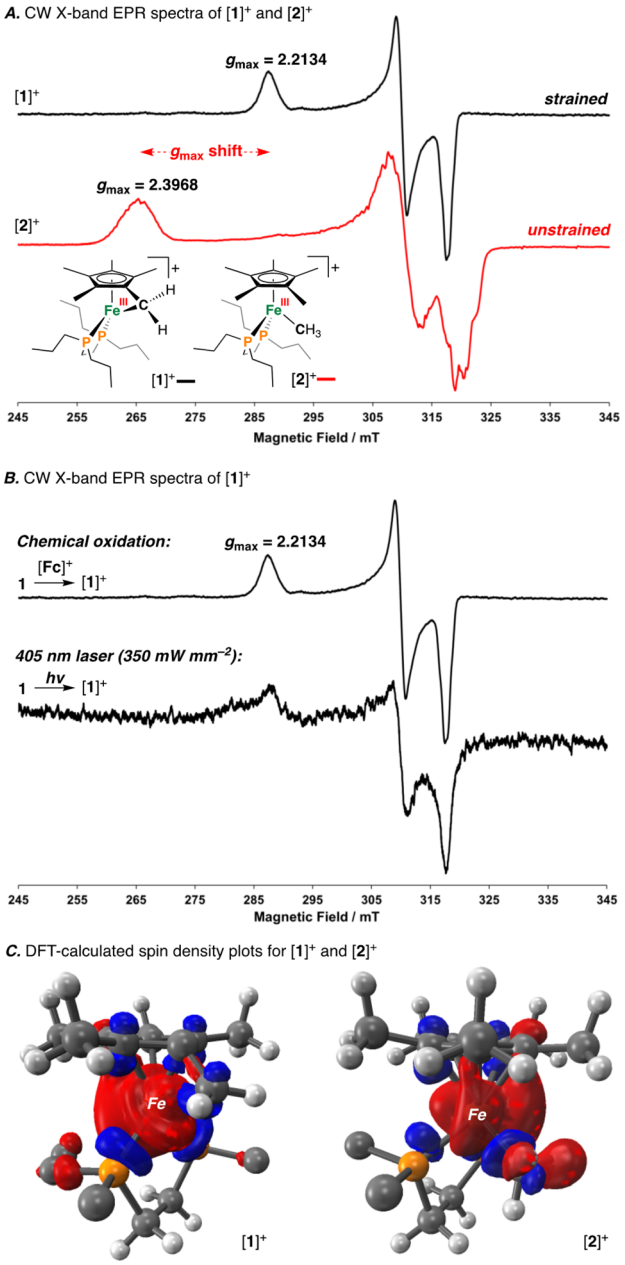

Fig. 5 A) Freeze-quenched CW X-band EPR spectra (8.885 GHz) recorded in 2-MeTHF glass at 77 K for [**1**]$^+$ (black) and [**2**]$^+$ (red). (B) Freeze-quenched CW X-band EPR spectra for [**1**]$^+$ (top) and a photo-oxidized sample of **1** under 405 nm (350 mW mm^{-2}) irradiation (bottom). (C) DFT-calculated spin-density plots for [**1**]$^+$ and [**2**]$^+$ (all C and H atoms from the d*n*ppe ligand, except those C atoms directly attached to P, have been omitted for clarity). Fc = Cp_2Fe.

a larger value of g_{max} is consistent with an unpaired electron residing in a $d_{x^2-y^2}$ orbital.[49] Calculated spin density plots for $[\mathbf{1}]^+$ and $[\mathbf{2}]^+$ additionally corroborate that the unpaired electron predominately resides on Fe, with populations of $0.917e^-$ for $[\mathbf{1}]^+$ and $0.987e^-$ for $[\mathbf{2}]^+$ (Fig. 5C). The marked geometry change noted above (between $[\mathbf{1}]^+$ and $[\mathbf{2}]^+$) is best visualized from an overlay plot of their DFT-optimized structures (with coincident Fe and P atoms) (Fig. 6A). This data also showcases an elongated Fe–C bond in $[\mathbf{1}]^+$ (d(Fe–C) = 2.24 Å) as compared to $[\mathbf{2}]^+$ (d(Fe–C) = 2.01 Å), indicating weaker Fe–C overlap in $[\mathbf{1}]^+$. The ring-strain inherent to $[\mathbf{1}]^+$ is additionally described by an Fe–C–C triangle with angles of 38.4°, 60.5°, and 81.1° (Fig. 6A).

Mayer bond order (MBO) and natural bond orbital (NBO) analysis provide further insight that helps to rationalize $C(sp^3)$–$C(sp^3)$ coupling in $[\mathbf{1}]^+$ (Fig. 6B).[50] To determine the change in bond order upon oxidation, MBOs were calculated. For $\mathbf{1}/[\mathbf{1}]^+$, the MBO decreased by 0.06 on oxidation ($\mathbf{1}$: 0.66/$[\mathbf{1}]^+$: 0.60), while for $\mathbf{2}/[\mathbf{2}]^+$, the MBO was found to slightly increase ($\mathbf{2}$: 0.73/$[\mathbf{2}]^+$: 0.80). NBO calculations provided second order perturbation energies ($E^{(2)}$) which showed a similar trend. For the C(lp) → Fe(lv) (lp = lone pair, lv = lone valence) interaction, energies were found to be 43.4 and 53.8 kcal mol^{-1} for $[\mathbf{1}]^+$ and $[\mathbf{2}]^+$, respectively (Fig. 6B). This data indicates that (1) the Fe–C bond becomes weaker on going from $\mathbf{1}$ → $[\mathbf{1}]^+$ and (2) that the Fe–C bond of $\mathbf{1}/[\mathbf{1}]^+$ is weaker than $\mathbf{2}/[\mathbf{2}]^+$ – a consequence of ring-strain.

The radical character intrinsic to $[\mathbf{1}]^+$ is also evidenced by its chemical reactivity with 10 equiv. of the radical trap, (2,2,6,6-tetramethylpiperidin-1-yl)oxyl (TEMPO), which gives $[\{\eta^5\text{-}C_5Me_4\text{–}(CH_2\text{–}ONC_9H_{18})\}Fe^{II}(dnppe)(NCCH_3)]B(C_6F_5)_4$ ($[\mathbf{8}]B(C_6F_5)_4$) (Fig. 6C). Compound $[\mathbf{8}]^+$ was characterized by signals in the ^{1}H NMR spectrum corresponding to $\{CH_2\text{–}ONC_9H_{18}\}$ at δ_H = 4.18 ppm and Fe-bound $NCCH_3$ at δ_H = 2.40 ppm. Confirmation of an Fe-bound $NCCH_3$ group was determined *via* FT-IR spectroscopy, with a characteristic ν(N≡C) stretch at 2247 cm^{-1}. The $^{13}C\{^1H\}$ NMR spectrum also showed a signal at δ_C = 71.0 ppm, corresponding to the TEMPO-bound CH_2 from the $\eta^5\text{-}C_5Me_4\text{–}(CH_2\text{–}ONC_9H_{18})$ ligand. HRMS-ESI also provided a signal corresponding to $[\mathbf{8}]^+$ at 649.407 (calcd; 649.407). These

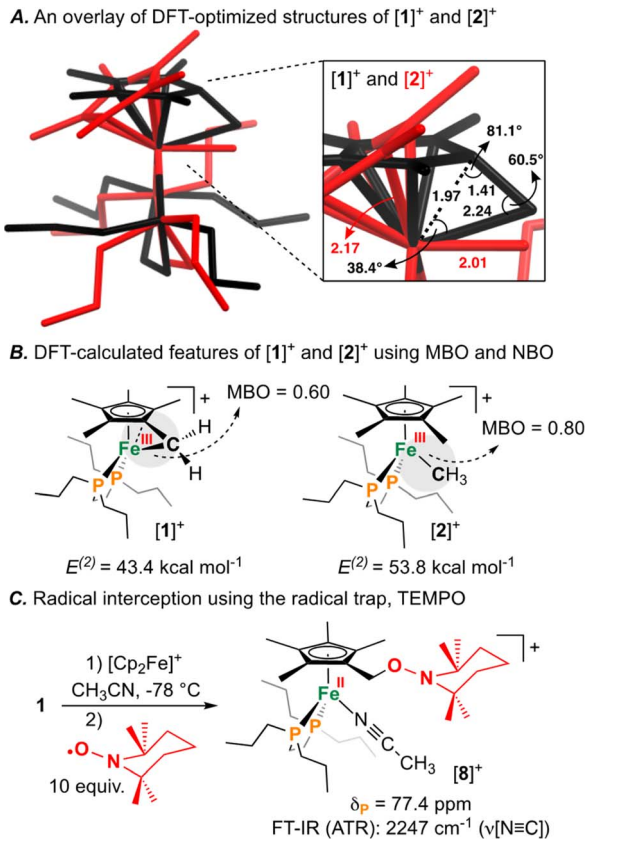

Fig. 6 (A) Structural overlay (capped sticks) of $[\mathbf{1}]^+$ (black) and $[\mathbf{2}]^+$ (red). Select angles (°) and select bond lengths (Å) are provided. (B) Mayer bond order (MBO) and natural bond orbital (NBO) analysis providing $E^{(2)}$ values between [Fe]–C. (C) Reaction of $[\mathbf{1}]^+$ with (2,2,6,6-tetramethylpiperidin-1-yl)oxyl (TEMPO) forming $[\mathbf{8}]^+$.

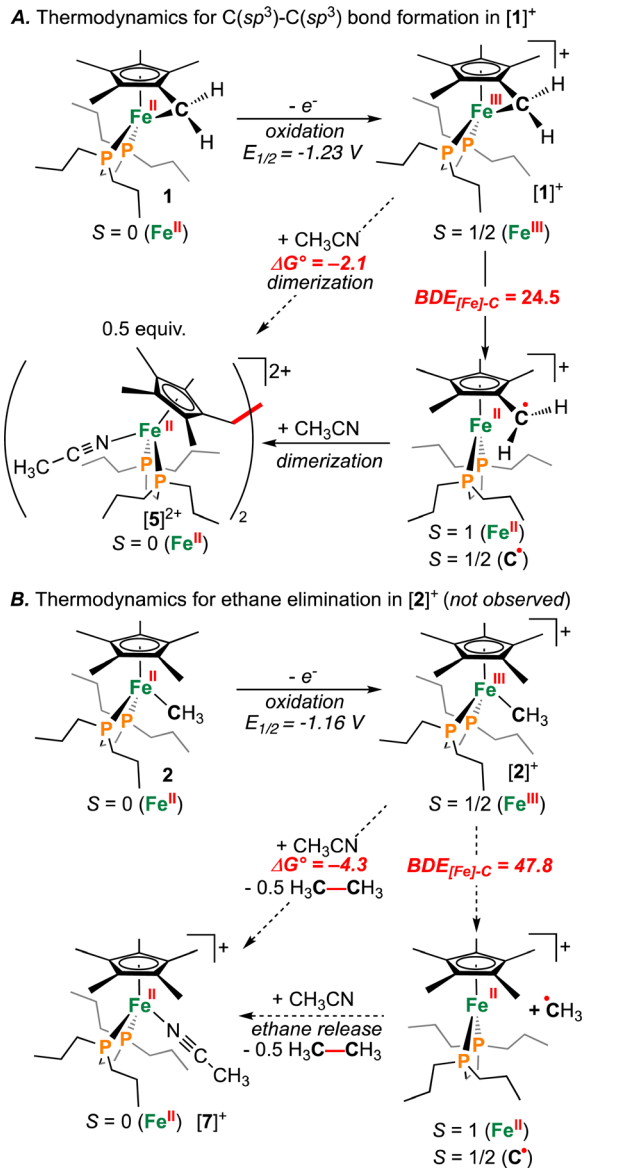

Fig. 7 (A) Thermodynamic calculations showing energies associated with the dimerization of $[\mathbf{1}]^+$. (B) Analogous calculations for the elimination of ethane (CH_3CH_3) from $[\mathbf{2}]^+$. All energies are in kcal mol^{-1}.

data corroborate a radical mechanism, whereby the generated {C_5Me_4–($\cdot CH_2$)} group has been trapped by TEMPO.[51]

To assess the effect of ring-strain on {[Fe]–C} bond homolysis, we next sought information regarding the $BDE_{[Fe]-C}$ of $[\mathbf{1}]^+$. For reference, the BDE_{C-C} associated with the simplest cyclical saturated hydrocarbon (cyclopropane; $(CH_2)_3$) is substantially lower than ethane due to ring strain ($BDE_{C-C(cyclopropane)}$ = 57 kcal mol^{-1} *vs.* $BDE_{C-C(ethane)}$ = 90 kcal mol^{-1}).[52–54] Given this, and assuming CH_3CH_3 and RCH_2CH_2R (R = $C_5Me_4^-$) to have similar bond strengths, C–C coupling should be favoured for {[Fe]–CH_2R} when $BDE_{[Fe]-C} \leq$ 45 kcal mol^{-1}.

Computations show the difference in $BDE_{[Fe]-C}$ for $[\mathbf{1}]^+$ and $[\mathbf{2}]^+$ to be 23.3 kcal mol^{-1} (Fig. 7). The absolute values of $BDE_{[Fe]-C}$: 24.5 and 47.8 kcal mol^{-1} for $[\mathbf{1}]^+$ and $[\mathbf{2}]^+$, respectively are also consistent with observation of C(sp^3)–C(sp^3) coupling for the former. These calculated values are benchmarked against ethane, which provides BDE_{C-C}(calcd) = 88.4 kcal mol^{-1} *c.f.*, the experimental BDE_{C-C} = 90 kcal mol^{-1}.[52] Notwithstanding differences in BDE_{C-C}, both processes were calculated to be mildly exergonic (Fig. 7): $\Delta G°$ = −2.1 kcal mol^{-1} and −4.3 kcal mol^{-1} for C–C coupling from $[\mathbf{1}]^+$ or $[\mathbf{2}]^+$, respectively, suggesting a difference in kinetic barrier. Based on the above discussion, the C(sp^3)–C(sp^3) coupling associated with $[\mathbf{1}]^+$ can thus be ascribed to a minimum of two features: (1) a strained three-membered {–Fe–CH_2–C–} ring and (2) a weakened {[Fe^{III}]–CH_2R} bond *c.f.*, **1**.[32] This is contrasted with $[\mathbf{2}]^+$, where experimentally, CH_3CH_3 is not evolved during synthesis (Fig. 7B).

Conclusions

Metal-mediated cross-coupling has emerged as a powerful means to construct C–C bonds. In recent years, such studies have focused predominantly on base transition elements, such as iron, cobalt, and nickel, as cheaper and more sustainable sources. Here, we have studied an oxidized iron tucked-in complex [(η^6-C_5Me_4=CH_2)Fe^{III}(d*n*ppe)]$^+$ ($[\mathbf{1}]^+$), which due to both ring-strain and iron oxidation state, promotes C(sp^3)–C(sp^3) bond coupling. The product {Fe_2} diphosphine dimers invite reactions to give functionalized {Fe_2^{III}} or {Fe_2^{II}} products having coordinated halide, hydride, or solvent equivalents. Characterization of the reactive oxidized "tucked-in" {Fe^{III}} precursor was performed using CW X-band EPR spectroscopy, with computations revealing a weak {[$Fe]^{III}$–C} bond with $BDE_{[Fe]-C}$ = 24.5 kcal mol^{-1}. The observed C(sp^3)–C(sp^3) coupling, however, is not simply an artifact of iron oxidation state. The model, [Cp*Fe^{III}(d*n*ppe)(CH_3)]$^+$ $[\mathbf{2}]^+$, for instance, does not undergo C(sp^3)–C(sp^3) coupling, consistent with a higher calculated $BDE_{[Fe]-C}$ of 47.8 kcal mol^{-1}. This pair of compounds and their contrasting thermochemistry/reactivity pave the way towards better understanding the intricacies of {M–C} strain and metal oxidation state on reductive elimination, offering insight into an important elementary transformation of direct relevance to C–C bond coupling.

Data availability

The data supporting this article have been included as part of the ESI.† Crystallographic data for 4 has been deposited at the CCDC under 2341812. This data can be obtained free of charge from the cambridge crystallographic data centre *via* **www.ccdc.cam.uk/data_request/cif**.

Author contributions

Joseph A. Zurakowski: investigation, methodology, formal Analysis, visualization, writing – original draft, writing – review & editing. Connor S. Durfy: investigation, validation. Noah B. Stocek: investigation, methodology. Giovanni Fanchini: resources, methodology, funding acquisition. Marcus W. Drover: project administration, funding acquisition, visualization, supervision, formal analysis, conceptualization, methodology, writing – review & editing.

Conflicts of interest

There are no conflicts to declare.

Acknowledgements

The authors are grateful to Western University, the Council of Ontario Universities for a John C. Polanyi award to M. W. D., the Canadian Foundation for Innovation (LOF-212442), and the Natural Sciences and Engineering Research Council of Canada (Discovery Grant, RGPIN-2020-04480 (M. W. D.), RGPIN-2020-05008 (G. F.), Discovery Launch Supplement, DGECR-2020-00183), and graduate award (CGS-D/NSERC Vanier to J. A. Z.) for funding.

References

1 R. H. Grubbs, *Angew. Chem., Int. Ed.*, 2006, **45**, 3760–3765.
2 C. C. C. Johansson Seechurn, M. O. Kitching, T. J. Colacot and V. Snieckus, *Angew. Chem., Int. Ed.*, 2012, **51**, 5062–5085.
3 A. Biffis, P. Centomo, A. Del Zotto and M. Zecca, *Chem. Rev.*, 2018, **118**, 2249–2295.
4 B. Zhang, Y. Gao, Y. Hioki, M. S. Oderinde, J. X. Qiao, K. X. Rodriguez, H.-J. Zhang, Y. Kawamata and P. S. Baran, *Nature*, 2022, **606**, 313–318.
5 Y. Liu, P. Li, Y. Wang and Y. Qiu, *Angew. Chem., Int. Ed.*, 2023, **62**, e202306679.
6 P. Li, G. Kou, T. Feng, M. Wang and Y. Qiu, *Angew. Chem., Int. Ed.*, 2023, **62**, e202311941.
7 Y. Wang, S. Dana, H. Long, Y. Xu, Y. Li, N. Kaplaneris and L. Ackermann, *Chem. Rev.*, 2023, **123**, 11269–11335.
8 C. K. Prier, D. A. Rankic and D. W. C. MacMillan, *Chem. Rev.*, 2013, **113**, 5322–5363.
9 C.-S. Wang, P. H. Dixneuf and J.-F. Soulé, *Chem. Rev.*, 2018, **118**, 7532–7585.
10 M. De Abreu, P. Belmont and E. Brachet, *Eur. J. Org Chem.*, 2020, **2020**, 1327–1378.
11 L. K. G. Ackerman, J. I. Martinez Alvarado and A. G. Doyle, *J. Am. Chem. Soc.*, 2018, **140**, 14059–14063.
12 M. L. Clapson, C. S. Durfy, D. Facchinato and M. W. Drover, *Cell Rep. Phys. Sci.*, 2023, **4**, 101548.

13 X. Chen, K. M. Engle, D. Wang and J. Yu, *Angew. Chem., Int. Ed.*, 2009, **48**, 5094–5115.
14 M. B. Watson, N. P. Rath and L. M. Mirica, *J. Am. Chem. Soc.*, 2017, **139**, 35–38.
15 J. Kim, K. Shin, S. Jin, D. Kim and S. Chang, *J. Am. Chem. Soc.*, 2019, **141**, 4137–4146.
16 A. Cizikovs, E. E. Basens, P. A. Zagorska, A. Kinens and L. Grigorjeva, *ACS Catal.*, 2024, **14**, 1690–1698.
17 A. Pedersen and M. Tilset, *Organometallics*, 1993, **12**, 56–64.
18 W. Lau, J. C. Huffman and J. K. Kochi, *Organometallics*, 1982, **1**, 155–169.
19 M. P. Lanci, M. S. Remy, W. Kaminsky, J. M. Mayer and M. S. Sanford, *J. Am. Chem. Soc.*, 2009, **131**, 15618–15620.
20 K. Shin, Y. Park, M.-H. Baik and S. Chang, *Nat. Chem.*, 2018, **10**, 218–224.
21 T. J. Kealy and P. L. Pauson, *Nature*, 1951, **168**, 1039–1040.
22 P. J. Chirik, *Organometallics*, 2010, **29**, 1500–1517.
23 P. Preethalayam, K. S. Krishnan, S. Thulasi, S. S. Chand, J. Joseph, V. Nair, F. Jaroschik and K. V. Radhakrishnan, *Chem. Rev.*, 2017, **117**, 3930–3989.
24 A. Z. Kreindlin, F. M. Dolgushin, A. I. Yanovsky, Z. A. Kerzina, P. V. Petrovskii and M. I. Rybinskaya, *J. Organomet. Chem.*, 2000, **616**, 106–111.
25 E. I. Fedin, A. L. Blumenfeld, P. V. Petrovskii, A. Z. Kreindlin, S. S. Fadeeva and M. I. Rybinskaya, *J. Organomet. Chem.*, 1985, **292**, 257–268.
26 A. Z. Kreindlin, S. S. Fadeeva and M. I. Rybinskaya, *Izv. Akad. Nauk SSSR, Ser. Khim.*, 1984, **2**, 403–406.
27 J. A. Zurakowski and M. W. Drover, *Chem. Commun.*, 2023, **59**, 11349–11352.
28 J. P. Dinnocenzo, W. P. Todd, T. R. Simpson and I. R. Gould, *J. Am. Chem. Soc.*, 1990, **112**, 2462–2464.
29 P. Peng, X. Yan, K. Zhang, Z. Liu, L. Zeng, Y. Chen, H. Zhang and A. Lei, *Nat. Commun.*, 2021, **12**, 3075.
30 T. Krämer, M. R. Gyton, I. Bustos, M. J. G. Sinclair, S. Tan, C. J. Wedge, S. A. Macgregor and A. B. Chaplin, *J. Am. Chem. Soc.*, 2023, **145**, 14087–14100.
31 Given the similarity of $E_{1/2}$ for both **1** and **2**, along with the lower reduction potentials ($E_{1/2} \ll -1.23$ V *vs.* Fc/Fc$^+$) observed for related Fe(0) species, a formal Fe(II) oxidation state seemingly better describes the observed electrochemical behaviour of **1**.
32 M. Tilset, I. Fjeldahl, J.-R. Hamon, P. Hamon, L. Toupet, J.-Y. Saillard, K. Costuas and A. Haynes, *J. Am. Chem. Soc.*, 2001, **123**, 9984–10000.
33 D. Patel, A. Wooles, A. D. Cornish, L. Steven, E. S. Davies, D. J. Evans, J. McMaster, W. Lewis, A. J. Blake and S. T. Liddle, *Dalton Trans.*, 2015, **44**, 14159–14177.
34 J. A. Zurakowski, K. R. Brown and M. W. Drover, *Inorg. Chem.*, 2023, **62**, 7053–7060.
35 Complex **1** is insoluble in pure acetonitrile and was found to react with CH_2Cl_2.
36 F. S. Pick, D. B. Leznoff and M. D. Fryzuk, *Dalton Trans.*, 2018, **47**, 10925–10931.
37 P. Hamon, L. Toupet, J.-R. Hamon and C. Lapinte, *Organometallics*, 1996, **15**, 10–12.
38 Y. Liu, E. Solari, R. Scopelliti, F. Fadaei Tirani and K. Severin, *Chem.–Eur. J.*, 2018, **24**, 18809–18815.
39 M. Kessler, S. Hansen, C. Godemann, A. Spannenberg and T. Beweries, *Chem.–Eur. J.*, 2013, **19**, 6350–6357.
40 X. Tan, B. Li, S. Xu, H. Song and B. Wang, *Organometallics*, 2013, **32**, 3253–3261.
41 F. Wochner, L. Zsolnai, G. Huttner and H. H. Brintzinger, *J. Organomet. Chem.*, 1985, **288**, 69–77.
42 D. V. Muratov, A. S. Romanov, M. Corsini, A. R. Kudinov, F. F. de Biani and W. Siebert, *Chem.–Eur. J.*, 2017, **23**, 11935–11944.
43 X. Wang, M. Sabat and R. N. Grimes, *Organometallics*, 1995, **14**, 4668–4675.
44 Y. Kwon, C. Lee and S. Park, *Chem. Phys.*, 2014, **445**, 38–45.
45 B. Dereka, N. H. C. Lewis, J. H. Keim, S. A. Snyder and A. Tokmakoff, *J. Phys. Chem. B*, 2022, **126**, 278–291.
46 E. S. Wiedner, M. B. Chambers, C. L. Pitman, R. M. Bullock, A. J. M. Miller and A. M. Appel, *Chem. Rev.*, 2016, **116**, 8655–8692.
47 J. Morrow, D. Catheline, M. H. Desbois, J. M. Manriquez, J. Ruiz and D. Astruc, *Organometallics*, 1987, **6**, 2605–2607.
48 D. Chong, W. E. Geiger, N. A. Davis, A. Weisbrich, Y. Shi, A. M. Arif and R. D. Ernst, *Organometallics*, 2008, **27**, 430–436.
49 F. Paul and C. Lapinte, *Coord. Chem. Rev.*, 1998, **178–180**, 431–509.
50 A. J. Bridgeman, G. Cavigliasso, L. R. Ireland and J. Rothery, *J. Chem. Soc., Dalton Trans.*, 2001, 2095–2108.
51 Of note, complexes **1** and **2** exhibited no reactivity with TEMPO.
52 B. Ruscic, *J. Phys. Chem. A*, 2015, **119**, 7810–7837.
53 F. H. Seubold, *J. Phys. Chem.*, 1954, **22**, 945–946.
54 X. Lei, X. Cao, J. Wang and X. Li, *Combust. Flame*, 2022, **237**, 111881.